SAND REPORT

SAND2003-1048
Unlimited Release
Printed April 2003

CavityExpansion: A Library for Cavity Expansion Algorithms, Version 1.0

Kevin H. Brown, J. Richard Koteras, Don B. Longcope, and Thomas L. Warren

Prepared by
Sandia National Laboratories
Albuquerque, New Mexico 87185 and Livermore, California 94550

Sandia is a multiprogram laboratory operated by Sandia Corporation,
a Lockheed Martin Company, for the United States Department of Energy's
National Nuclear Security Administration under Contract DE-AC04-94-AL85000.

Issued by Sandia National Laboratories, operated for the United States Department of Energy by Sandia Corporation.

Available to DOE and DOE contractors from
U.S. Department of Energy
Office of Scientific and Technical Information
P.O. Box 62
Oak Ridge, TN 37831

Telephone: (865)576-8401
Facsimile: (865)576-5728
E-Mail: reports@adonis.osti.gov
Online ordering: http://www.doe.gov/bridge

Available to the public from
U.S. Department of Commerce
National Technical Information Service
5285 Port Royal Rd
Springfield, VA 22161

Telephone: (800)553-6847
Facsimile: (703)605-6900
E-Mail: orders@ntis.fedworld.gov
Online order: http://www.ntis.gov/help/ordermethods.asp?loc=7-4-0#online

SAND2003-1048
Unlimited Release
Printed April 2003

CavityExpansion: A Library for Cavity Expansion Algorithms, Version 1.0

Kevin H. Brown
Computation, Computers, Information, and Mathematics Center

J. Richard Koteras and Don B. Longcope
Engineering Sciences Center

Thomas L. Warren
Aerospace Systems Development Center

Sandia National Laboratories
Box 5800
Albuquerque, NM 87195-0847

Abstract

Cavity expansion is a method for modeling the penetration of an axisymmetric or wedge-shaped solid body—a penetrator—into a target by using analytic expressions to capture the effects of the target on the body. Cavity expansion has been implemented as a third-party library (CavityExpansion) that can be used with explicit, transient dynamics codes. This document describes the mechanics of the cavity expansion model implemented as a third-party library. This document also describes the applications interface to CavityExpansion. A set of regression tests has been developed that can be used to test the implementation of CavityExpansion in a transient dynamics code. The mechanics of these tests and the expected results from the tests are described in detail.

Acknowledgments

The authors would like to thank Tom Voth and Gerald Wellman for their review of this document. The authors would also like to thank Rhonda Reinert of Technically Write for her careful review and editing of this document and her many valuable suggestions for improving the organization and clarity of this document.

Contents

Figures

Intentionally Left Blank

CavityExpansion: A Library for Cavity Expansion Algorithms, Version 1.0

1 Introduction

Cavity expansion is a method for modeling the penetration of an axisymmetric or wedge-shaped solid body (a penetrator) into a target by using analytic expressions to capture the effects of the target on the penetrator. The advantage of this approach is that the target does not need to be discretized. The characteristics of the target are captured by coefficients in an equation that is used to determine a pressure load on the penetrator. The pressure load at a point on the penetrator depends on the geometry of the penetrator at that point and the velocity of that point.

Cavity expansion has been implemented as a third-party library, named CavityExpansion, that can be used in explicit, transient dynamics codes. This document describes the implementation of the cavity expansion functionality and the applications interface to CavityExpansion. This document also discusses verification and validation of CavityExpansion as a third-party library.

The theoretical background for cavity expansion can be found in References 2, 4, 5, 6, 7, and 9. References 10, 11, 12, and 16 describe how cavity expansion has been implemented as a specialized boundary condition in two widely used finite element codes, Pronto3d [13] and ABAQUS Explicit [1], and used for comparison of computational results with experiments.

Highlights of this document follow:

- Section 2 describes the implementation of the current functionality in CavityExpansion. Section 2.1 provides the basic information required for the numerical implementation of cavity expansion. Sections 2.2 and 2.3 discuss the two special cases of cavity expansion theory, spherical and cylindrical, respectively. Section 2.4 explains how the basic theory for cavity expansion can be enhanced for a numerical implementation by accounting for what are called free-surface effects.
- Section 3 describes the applications interface for CavityExpansion.
- Section 4 gives a complete description of the set of verification problems used to test the current functionality in CavityExpansion.
- Section 5 references a set of validation problems for cavity expansion.
- Appendix A gives the basic algorithm flow used for the implementation of cavity expansion.

The CavityExpansion library is currently used by Alegra [3] and Presto[8].

2 Implementation

This section describes the current numerical implementation of cavity expansion capabilities in the third-party library CavityExpansion.

2.1 Pressure Equation

A typical penetrator and target are shown in Figure 2.1.

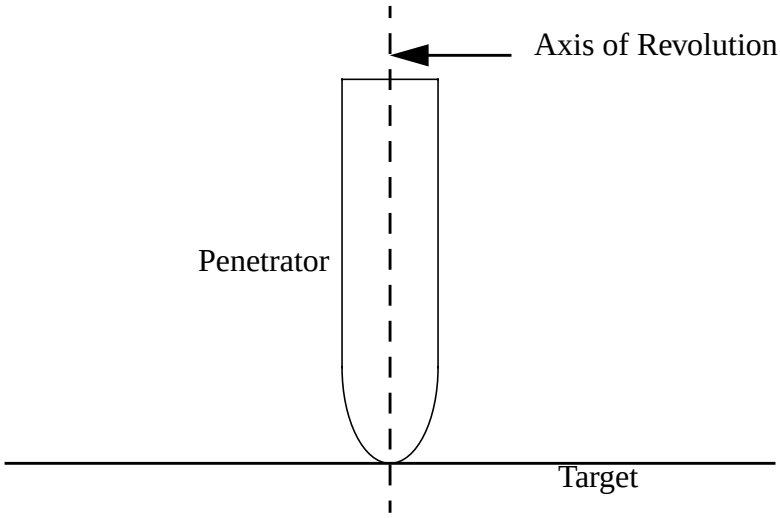

Figure 2.1. Axisymmetric penetrator normal to target surface.

The pressure at some point on the surface of the penetrator is determined from cavity expansion theory by a quadratic equation of the form

$$p = c_0 + c_1 v + c_2 v^2, \tag{1}$$

where v is a velocity of a particle in the target. The particle is in contact with the point of interest on the surface of the penetrator. The three coefficients in Equation (1), c_0, c_1, and c_2, reflect the properties of the target. For a given target material, these three parameters are usually determined from experiments. Cavity expansion is typically used for axisymmetric bodies, but it can also be applied to wedge-shaped bodies.

In a numerical implementation of cavity expansion, the axisymmetric body (penetrator) is modeled with a mesh. The surface of the body where the effects of cavity expansion occur is modeled by a set of faces, and outward normals can be calculated on these faces. The axis of revolution of the body can be defined by a minimum of two points on the axis. If the body does not undergo significant bending, two points are sufficient to model the location of the axis of revolution of the body as the body impacts a target. If, however, the

body undergoes significant bending, the axis of revolution should be broken into a series of segments (each segment defined by two points) to provide accurate modeling.

For problems involving cavity expansion, it is necessary to specify the location and depth of the target relative to the penetrator. For some problems, the depth of the target is finite; for other problems the target may be a semi-infinite medium. The bounds of the target are referred to as the free surfaces. The convention is to have these surfaces normal to one of the global coordinate axes—X, Y, or Z. The normal to the top surface is in the positive direction of one of the global coordinate axes. The surfaces are then specified by points on the global axis normal to the surfaces of the target. For example, suppose the normal to the top surface of the target is in the +*z*-direction and the target is 10 m thick. The top of the target lies in the *xy*-plane; the bottom of the target is at $z = -10$ m. For this particular problem, the top free surface would be specified as $z = 0$, and the bottom free surface would be specified as $z = -10$. For a semifinite medium, it is possible to specify a large-enough depth so that the penetrator never leaves the target during the computational period of interest. For the CavityExpansion library, the *z*-axis has been chosen as the normal to the target for all problems. The model for any penetrator can be easily oriented to account for this convention.

The model of the body (with points defining the axis of revolution) and the specification of the target provide the basic information needed for an analysis using a cavity expansion method. The velocity term in Equation (1) can be computed by one of two methods, spherical expansion or cylindrical expansion. These two methods make different assumptions about the motion of particles in the target. For spherical cavity expansion, it is assumed that target particles contacting the surface of the penetrator move normal to the surface of the penetrator. For cylindrical cavity expansion, it is assumed that target particles contacting the surface of the penetrator move in a direction that is normal to the axis of the penetrator. These two types of target particle motion are shown in Figure 2.2.

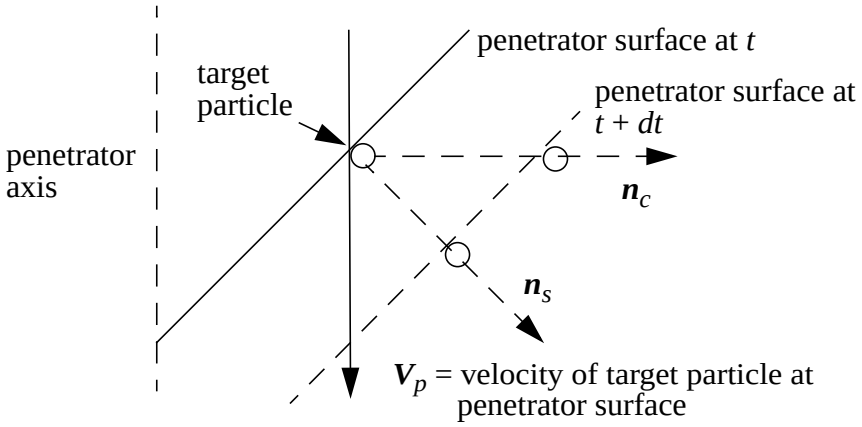

Figure 2.2. Target particle motion for spherical and cylindrical expansion.

In Figure 2.2, the normal for spherical expansion is denoted as $\boldsymbol{n}_c$, and the normal for cylindrical expansion is denoted as $\boldsymbol{n}_s$.

Section 2.2 discusses the details of computing v using spherical expansion theory, and Section 2.3 discusses the details of computing v with cylindrical expansion theory.

When cavity expansion is implemented as a numerical scheme, it is necessary to account for the fact that the surface of the penetrator is no longer a smooth surface but a series of planar facets. These facets could be shell elements or the faces of hexahedral or tetrahedral elements. In the next sections concerning the implementation of spherical and cylindrical expansion, the effects of the discretization of the surface are noted.

2.2 Spherical Expansion

For the case of spherical cavity expansion, consider the geometry shown in Figure 2.3.

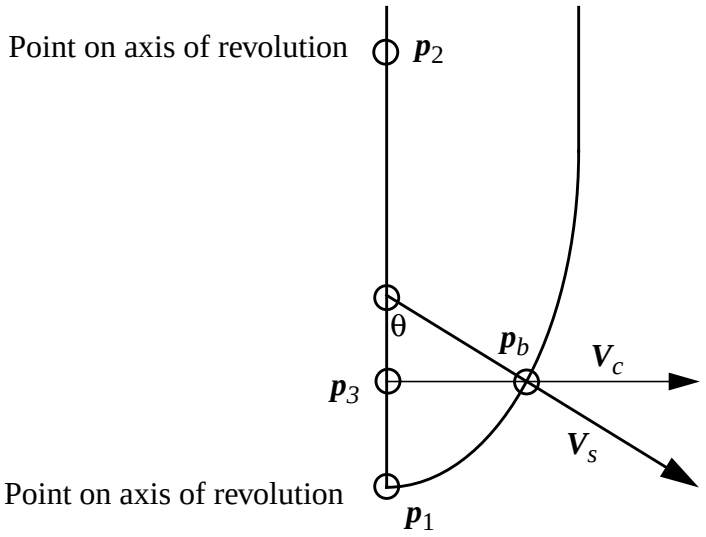

Figure 2.3. Spherical radii calculations.

The axis of revolution of the body is defined by points $\boldsymbol{p}_1$ and $\boldsymbol{p}_2$. (Because the points can be represented by vectors, we will denote them as vector quantities.) There are two quantities of interest for any point $\boldsymbol{p}_b$ on the surface of the penetrator. The first quantity of interest is the normal to the surface of the penetrator at $\boldsymbol{p}_b$; denote this normal as $\boldsymbol{V}_s$. The second quantity of interest is the spherical radius for the point $\boldsymbol{p}_b$. The spherical radius d_s for $\boldsymbol{p}_b$ is the distance from $\boldsymbol{p}_b$ to the axis of revolution of the body along the vector $\boldsymbol{V}_s$. This distance will be important for calculations of surface effects that are discussed in Section 2.4.

To compute the spherical distance, first compute a vector $\boldsymbol{A}$ that lies along the axis of revolution and extends from point $\boldsymbol{p}_2$ to point $\boldsymbol{p}_1$.

$$\boldsymbol{A} = \boldsymbol{p}_1 - \boldsymbol{p}_2 \tag{2}$$

Points $\boldsymbol{p}_2$ and $\boldsymbol{p}_1$ can be any two noncoincident points that lie on the axis of revolution. The point $\boldsymbol{p}_1$ should be toward the nose of the body, and the point $\boldsymbol{p}_2$ should be toward the aft end of the body.

Now compute a vector $\boldsymbol{B}$ from point $\boldsymbol{p}_2$ to $\boldsymbol{p}_b$.

$$\boldsymbol{B} = \boldsymbol{p}_b - \boldsymbol{p}_2 \tag{3}$$

If $\boldsymbol{a}$ is the unit vector corresponding to $\boldsymbol{A}$, then the point $\boldsymbol{p}_3$ can be computed from

$$\boldsymbol{p}_3 = (\boldsymbol{a} \cdot \boldsymbol{B})\boldsymbol{a} + \boldsymbol{p}_2. \tag{4}$$

Point $\boldsymbol{p}_3$ and point $\boldsymbol{p}_b$ define a vector that is orthogonal to the axis of revolution of the penetrator. Once point $\boldsymbol{p}_3$ is computed, it is possible to compute the distance, d_c, from $\boldsymbol{p}_3$ to point $\boldsymbol{p}_b$. By using $\boldsymbol{p}_3$, it is possible to compute the vector $\boldsymbol{V}_c$, which is the cylindrical normal through $\boldsymbol{p}_b$ (Figure 2.3). If $\boldsymbol{n}_c$ is the unit vector lying along $\boldsymbol{V}_c$, and $\boldsymbol{n}_s$ is the unit vector lying along $\boldsymbol{V}_s$, the value for the spherical distance d_s can be computed from

$$d_s = d_c / (\boldsymbol{n}_c \cdot \boldsymbol{n}_s) \tag{5}$$

provided that $\boldsymbol{n}_c \cdot \boldsymbol{n}_s \neq 0$. The condition $\boldsymbol{n}_c \cdot \boldsymbol{n}_s \neq 0$ may be violated at the tip of the penetrator as the surface of the body comes close to the axis of revolution. This situation is easy to detect, and one can use a user-specified value for the radius at the tip of the body to overcome the problem encountered with the above calculations. For a spherical expansion problem, a user-specified tip radius would have the effect of rounding the tip of a sharp nose, such as an ogival nose.

Note that in the preceding derivation, it is assumed that $\boldsymbol{V}_s$ lies in the plane defined by the vector $\boldsymbol{V}_c$ and the vector $\boldsymbol{B}$. For the discretized model of the penetrator, the vector $\boldsymbol{V}_s$ does NOT necessarily lie in the plane defined by $\boldsymbol{V}_c$ and $\boldsymbol{B}$. The following section describes the modified procedure to obtain d_s appropriate for the discrete penetrator model.

The above calculations offer a means of determining the spherical distance d_s associated with the spherical vector $\boldsymbol{V}_s$. The spherical vector $\boldsymbol{V}_s$ is determined from the discretized

geometry in the finite element model for the penetrator. Consider the discretized profile of a penetrator shown in Figure 2.4.

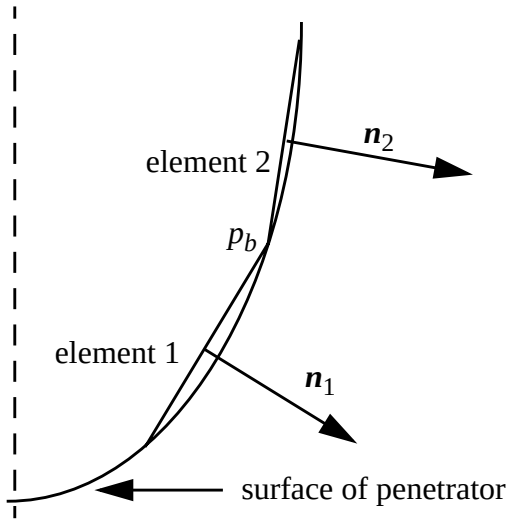

Figure 2.4. Discretized surface of penetrator.

In the profile in Figure 2.4, the line representing the surface of the penetrator has been broken into straight-line segments. These segments would result from slicing through hexahedral or tetrahedral elements with a plane that passes through the body of revolution. Consider the case of a quadrilateral face (Figure 2.5) arising from hexahedral elements used in a cavity expansion model.

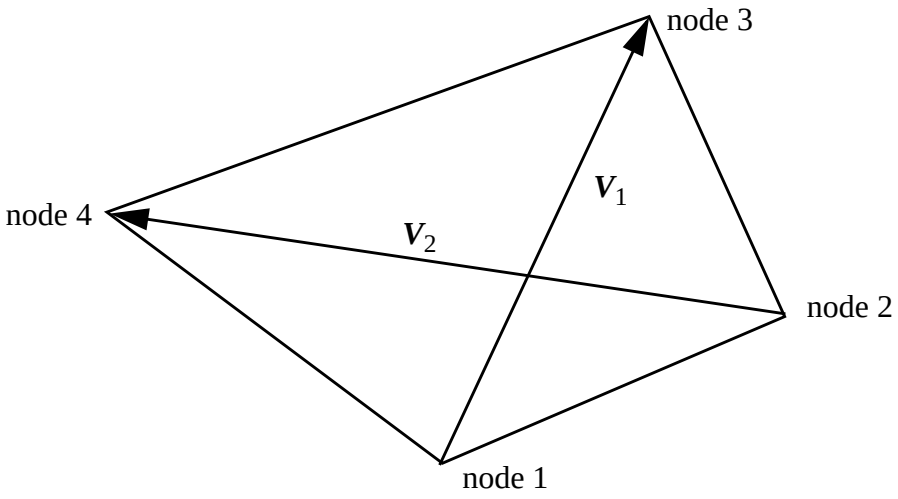

Figure 2.5. Quadrilateral face on surface of penetrator.

For a quadrilateral face, an average surface (spherical) normal is calculated. To calculate this average normal, a vector $\boldsymbol{V}_1$ is computed from node 1 to node 3, and a second vector

$\boldsymbol{V}_2$ is computed from node 2 to node 4. The cross product $\boldsymbol{V}_1 \times \boldsymbol{V}_2$ is used to compute the average normal for the surface. This average normal is used for the spherical normal.

Consider the point $\boldsymbol{p}_b$ shown in Figure 2.4. Let point $\boldsymbol{p}_b$ correspond to a node, node i, shared by elements 1 and 2. For element 1, there will be a single normal, but four velocity vectors (one at each node). At node i for element 1, the velocity v used in Equation (1) is

$$v = \boldsymbol{v}_i \cdot \boldsymbol{n}_s, \tag{6}$$

where $\boldsymbol{n}_s$ is the spherical normal for element 1 and $\boldsymbol{v}_i$ is the velocity vector at node i. For a quadrilateral face, there are four pressures calculated based on Equation (6). These pressures are then used to calculate nodal point forces for an element based on a nonuniform pressure distribution. At a given node on the mesh, the nodal point force is the resultant of the nodal point loads summed from surrounding elements. Nodal forces from element 2 would also be summed into the nodal forces at $\boldsymbol{p}_b$.

The discretization of the surface of the quadrilateral requires that a different method be used in the calculation of d_s from that given in Equation (5). Figure 2.6 shows the discretized cross section of a penetrator.

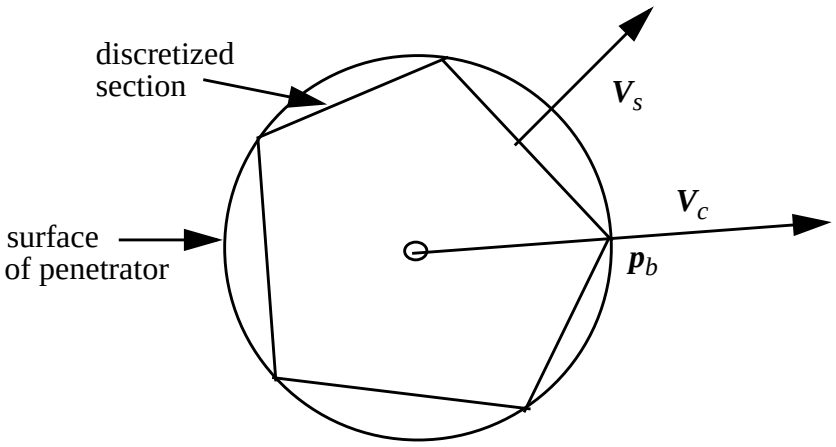

Figure 2.6. Cross section of penetrator.

The vector $\boldsymbol{V}_s$ does not lie in the same plane as that defined by the vector $\boldsymbol{V}_c$ and the axis of revolution of the body. The vector $\boldsymbol{V}_s$ only approximates the normal at $\boldsymbol{p}_b$. Since we want the spherical distance to the point on the body $\boldsymbol{p}_b$, it becomes necessary to project the unit vector lying along $\boldsymbol{V}_s$, which is $\boldsymbol{n}_s$, onto the plane defined by $\boldsymbol{V}_c$, the cylindrical normal, and $\boldsymbol{A}$, the axis of revolution of the body. If the unit vector lying along $\boldsymbol{A}$

(Equation (2)) is defined as $\boldsymbol{a}$, then the following operations will produce a good approximation of d_s that will get better as the penetrator mesh is refined.

$$\cos\theta = \left|\boldsymbol{n}_s \cdot \boldsymbol{a}\right| \tag{7}$$

$$\theta = \operatorname{acos}\left|\boldsymbol{n}_s \cdot \boldsymbol{a}\right| \tag{8}$$

$$d_c = d_s \sin\theta \tag{9}$$

$$d_s = d_c/(\sin\theta), \text{ for } \sin\theta \neq 0 \tag{10}$$

In the above equations, Equation (7) through Equation (10), θ is the angle between $\boldsymbol{a}$ and $\boldsymbol{n}_s$ projected onto the plane defined by $\boldsymbol{n}_c$ and $\boldsymbol{a}$. The angle θ is shown in Figure 2.3. Similar to the previous calculations for d_s, the above equations break down for nodes within a small distance of the tip. This problem can be corrected for the above calculations by again specifying a tip radius.

We now have sufficient information to compute the pressure for spherical cavity expansion for any node on the surface of a penetrator where cavity expansion effects are specified. For the case of spherical cavity expansion, the key equations are Equation (1) and Equation (6). If, in Equation (6), the value for v is less than zero (the velocity is in the opposite direction of the outward normal to the body), then the value for the pressure is set to zero.

2.3 Cylindrical Expansion

For the case of cylindrical expansion, again consider the geometry shown in Figure 2.3. The point $\boldsymbol{p}_3$, which lies on a line that passes through the point $\boldsymbol{p}_b$ and is normal to the axis of revolution of the body, can be calculated by using Equations (2) through (4). Once $\boldsymbol{p}_3$ is known, it is possible to calculate the vector $\boldsymbol{V}_c$ (and the related unit vector $\boldsymbol{n}_c$) and the distance d_c. The calculations break down for a point near the axis of revolution of the body. This is similar to the situation encountered in spherical expansion. If a point is encountered near the axis of revolution, a user-defined radius can be used at this point. If the tip of the penetrator is a hemispherical section (defined by a single radius of curvature), it is possible to use a user-specified value for a point at (or near) the tip of the penetrator that is equal to the radius of the hemispherical section. This gives continuity for the value of the cylindrical radius for all points in the hemispherical section.

The velocity quantity in Equation (1) for cylindrical expansion involves both the spherical and cylindrical vectors, $\boldsymbol{n}_s$ and $\boldsymbol{n}_c$. For a node i on a quadrilateral face, the velocity component in the direction of the spherical normal is first computed. Designate this dot product as v_{is}.

$$v_{is} = \boldsymbol{v}_i \cdot \boldsymbol{n}_s \tag{11}$$

The quantity v_{is} is then divided by the dot product $\boldsymbol{n}_c \cdot \boldsymbol{n}_s$. The quantity v in Equation (1) is defined as

$$v = v_{is} / (\boldsymbol{n}_c \cdot \boldsymbol{n}_s). \tag{12}$$

For cylindrical expansion, v is the radial expansion velocity component of the target at a point $\boldsymbol{p}_b$. We can better understand the physical significance of the radial velocity by considering the quantities shown in Figure 2.7. In this figure, the magnitude of the velocity at point $\boldsymbol{p}_b$ in the direction normal to the surface of the penetrator is

$$v_s = \boldsymbol{V}_p \cdot \boldsymbol{n}_s = \left\| \boldsymbol{V}_p \right\| \sin\phi, \tag{13}$$

where ϕ is the angle shown. The magnitude of the radial velocity of the material particle, v_c, is

$$v_c = \left\| \boldsymbol{V}_p \right\| \tan\phi = v_s / (\cos\phi). \tag{14}$$

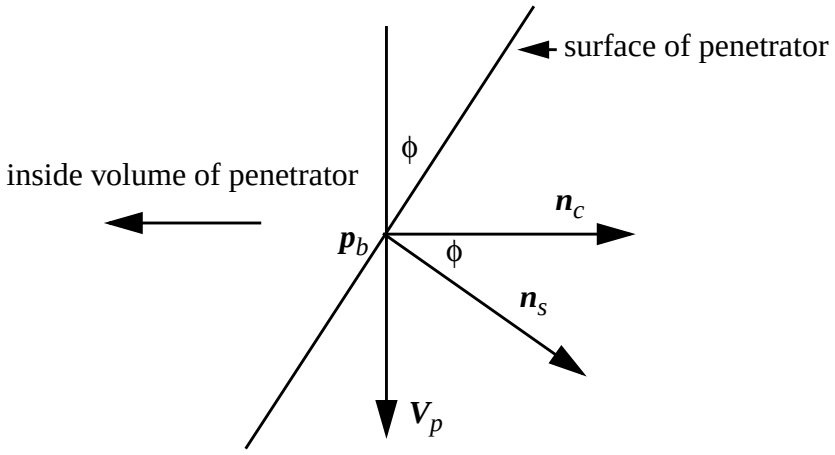

Figure 2.7. Relation between cylindrical and spherical velocities.

Equation (14) breaks down when $\cos\phi = 0$, which implies a blunt end to the penetrator. At a blunt end, there would be no unique direction for radial motion with respect to the axis of revolution. For this situation, the pressure is simply set to zero in Equation (1). (An analyst could use the spherical expansion technique for the "blunt" section of the body.) The pressure is also set to zero if the dot product between the velocity at a point on the body and the spherical normal is less than zero.

We now have sufficient information to compute the pressure for cylindrical cavity expansion for any node on the surface of a penetrator. For the case of cylindrical cavity

expansion, the key equations are Equation (1), Equation (11), and Equation (12). If, in Equation (12), the value for v is less than zero (the velocity is in the opposite direction of the cylindrical outward normal to the body), then the value for pressure is set to zero.

2.4 Free-Surface Effects

In some physical problems, the surface of a target may disintegrate easily near the impact zone. The penetrator will go into the target for some distance before the target remains intact and offers effective resistance to the penetrator. Cavity expansion in a finite element code can be implemented to take into account these surface effects.

Currently, only a simple on-off surface effect is implemented.

Surface effects are incorporated by using the free surfaces of the target and a layer definition. A single layer or several layers can reside inside the target, which is defined by the top and bottom free surfaces. The relation of a single layer to the target's free surfaces is shown in Figure 2.8. The single layer in the figure could consist of several layers (not

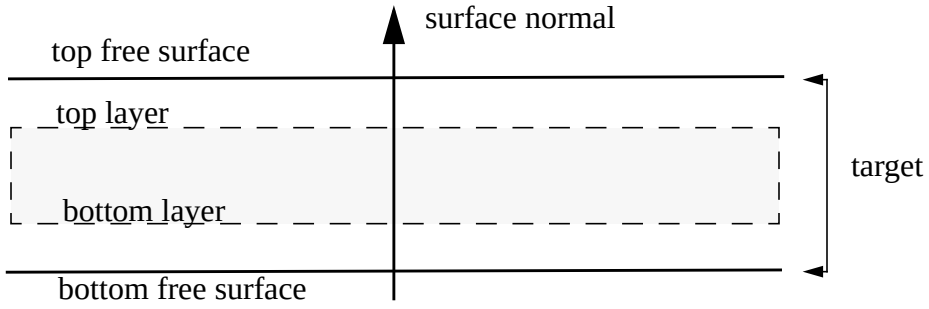

Figure 2.8. Target free surfaces and layer.

necessarily contiguous) with different properties. For the examples presented in the following section, we will assume a single layer resides within the target. In the computations for cavity expansion, a check is first made to determine whether a node on the surface of the penetrator lies within a layer. If the node lies outside of a layer, the pressure is set to zero for that node. If the node lies within the layer, then computations are made to determine a pressure derived from Equation (1).

If surface effects are important, information about the free surface is used to determine whether a node on the penetrator is sufficiently far from the free surface for a pressure to be applied according to Equation (1). For calculations of free-surface effects, consider the penetrator shown in Figure 2.9. It has entered the target at an oblique angle. A detailed example is presented for calculating the top free surface. Similar calculations will hold for the effects of the bottom free surface. The detailed example uses the case of spherical expansion. The same calculations for spherical expansion are easily generalized to the case of cylindrical expansion.

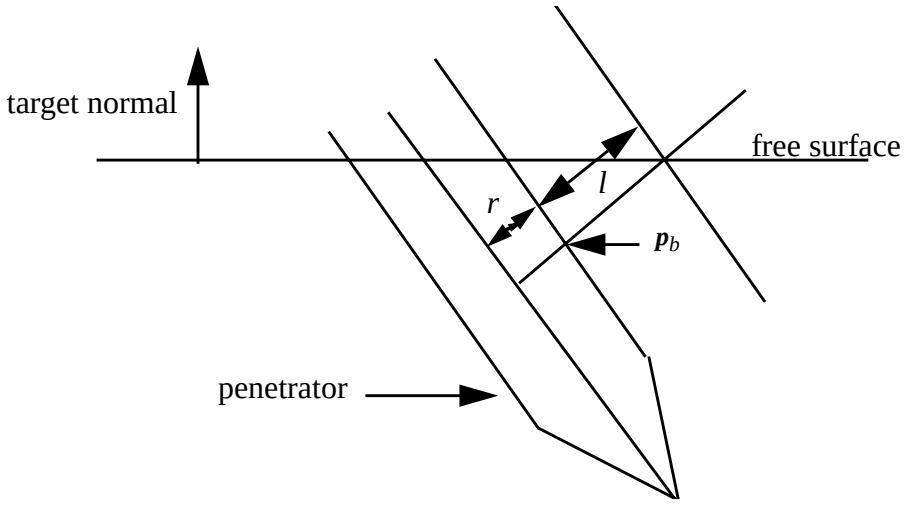

Figure 2.9. Geometry relations for calculations of surface effects.

Consider the point $\boldsymbol{p}_b$ on the surface of the penetrator for the case of spherical expansion. Point $\boldsymbol{p}_b$ is a distance r (spherical radius) from the axis of revolution of the penetrator. The distance from $\boldsymbol{p}_b$ to the target surface as measured along the spherical normal to the surface of the penetrator at $\boldsymbol{p}_b$ is l. If l and r satisfy the relation

$$l - f_s r > 0, \tag{15}$$

where f_s is a scale factor that characterizes the surface effects for a particular target, then a pressure will be calculated at $\boldsymbol{p}_b$ based on Equation (1). If Equation (15) is not satisfied, then the pressure is set to zero. Equation (15) is a simple test to determine whether a point on the body of the penetrator is far enough below the free surface of the target to have the material above the point remain intact. The larger the value of f_s, the farther a point on the penetrator must be below the top free surface if the point is to have a pressure from cavity expansion.

The scale factor f_s characterizes a critical ratio for l/r. The value for f_s varies for different materials. In subsequent sections, the scale factor f_s will be referred to as a surface effect coefficient.

The distance l is quite easy to compute. Suppose that point $\boldsymbol{p}_b$ is located at (x_b, y_b, z_b). The target normal for the top free surface is in the z-direction, and the top free surface is located at z_{fs}. If the spherical normal at point $\boldsymbol{p}_b$ is $\boldsymbol{n}_s = (n_{sx}, n_{sy}, n_{sz})$, then the distance l is simply

$$l = (z_{fs} - z_b)/n_{sz}, \tag{16}$$

for n_{sz} not equal to zero. The computation in Equation (16) is made only if n_{sz} is nonzero and is positive. If n_{sz} is positive, the spherical normal at $\boldsymbol{p}_b$ is pointing toward the top free surface, and it makes sense physically to check for the effects of the top free surface. If one of the other axes was normal to the top free surface, the values in Equation (16) would be changed to reflect this fact.

As indicated previously, the detailed analysis presented above for calculating the surface effects also applies to the case of cylindrical expansion. For the case of cylindrical expansion, we would use the cylindrical radius at $\boldsymbol{p}_b$ for r and compute l based on $\boldsymbol{n}_c$. The detailed analysis presented above also applies to the effects of the bottom free surface (with some sign changes).

3 Application Programmers Interface

This section describes the Application Programmers Interface (API). Currently, only a C++ interface is supported. A C and/or FORTRAN interface could easily be added in the future. The library does not have any parallel support built into it. The parallelization is left to the host code. All that is required is for the host code to “swap and add” the nodal forces to give a parallel implementation. Since any parallel code MUST provide this service for element assemblies, we have not added the coding in the library. There is no limit to the number of CavityExpansion objects that can be constructed.

Rather than use the namespace feature of C++, we have chosen to use a naming convention to avoid naming conflicts with the host code. The main-level object is named CavityExpansion. All other objects and enumerations are named with the prefix “CE_”. As long as the host code does NOT use “CE_” as a prefix for any of its objects, there should not be any name conflicts.

All of the functions in the CavityExpansion library return an error code given by the following enumeration:

```
CE_ERROR_CODE { NO_ERROR=0, INVALID_DATA, INTERNAL_ERROR };
```

The return error code should always be checked. As soon as the library detects an error, it exits. This can leave the object improperly initialized or the return data invalid. If the analysis is allowed to proceed after the library has returned an error code, the results are unpredictable but guaranteed to be wrong.

3.1 Constructing a CavityExpansion Object

There is one general-purpose constructor for the CavityExpansion object. There is no internal data needed for restart, so a general constructor can be used for restart as well.

The prototype for the CavityExpansion constructor is as follows:

```
CavityExpansion(
        CE_TYPE Type,
        int Number_Faces,
        int Number_Nodes,
        const int* Connectivity,
        double Tip_Radius,
        int Num_Layers,
        const double* Layer_Surface_Top,
        const double* Layer_Surface_Bottom,
        const int* Surface_Effect_Model_IDs,
        const double* Pressure_Coefficient_1,
        const double* Pressure_Coefficient_2,
        const double* Pressure_Coefficient_3,
        int Num_Body_Axis_Points,
        CavityExpansion::CE_ERROR_CODE& error );
```

Definitions of the input parameters are given below.

- The enumerate variable `Type` specifies the theory to use, and is one of the items in the enumerated list `CE_TYPE`.

```
enum CE_TYPE{ SPHERICAL, CYLINDRICAL };
```

- The integer `Number_Faces` is the number of faces to which the cavity expansion pressure needs to be computed.
- The integer `Number_Nodes` is the number of nodes needed to describe the connectivity for the faces.
- The array `Connectivity` describes the connectivity between the faces and the nodes. The first four integers in the array describe the connectivity for face 1; the second four integers describe the connectivity for face 2; and so forth. Only quadrilateral faces are allowed for the description of the surface used for cavity expansion.
- The real `Tip_Radius` gives the tip radius for the expansion radii described in Section 2.2 and Section 2.3.
- The integer `Num_Layers` is the number of layers used to describe the target space.
- The real array `Layer_Surface_Top` gives the location of the top surface for each of the `Num_Layers` layers.
- The real `Layer_Surface_Bottom` gives the location of the bottom surface for each of the `Num_Layers` layers.
- The integer array `Surface_Effect_Model_IDs` is the list of integer identifiers for the surface effect model for each layer. A value of zero indicates that no surface effect is to be used for this layer.
- The real array `Pressure_Coefficient_1` gives the pressure_coefficient_1 (c_0 in Equation 1 of Section 2.1) for each of the `Num_Layers` layers.
- The real array `Pressure_Coefficient_2` gives the pressure_coefficient_2 (c_1 in Equation 1 of Section 2.1) for each of the `Num_Layers` layers.
- The real array `Pressure_Coefficient_3` gives the pressure_coefficient_3 (c_2 in Equation 1 of Section 2.1) for each of the `Num_Layers` layers.
- The integer `Num_Body_Axis_Points` is the number of points that will be used to describe the body axis. In version 1.0, this must be two (2). In future versions, we will support an arbitrary number of body axis points so the analysts can better resolve the body axis.

3.2 Adding Surface Effect Models

Surface effect models are added using the function `Add_Surface_Effect_Model`. The prototype for this function is as follows:

```
CE_ERROR_CODE
```

```
CavityExpansion::Add_Surface_Effect_Model(
       CE_SURFACE_EFFECT_TYPE type,
       int ID,
       double* params );
```

Definitions of the input parameters are given below.

- The enumerated variable `type` specifies the surface effect model to use, and is one of the items from the enumated list `CE_SURFACE_EFFECT_TYPE`.

  ```
  enum CE_SURFACE_EFFECT_TYPE{ NONE=0, SIMPLE_ON_OFF};
  ```

- The integer `ID` is a POSITIVE integer for this model. This `ID` is used to connect the models to the layers. The `ID` used here should appear in the array `Surface_Effect_Model_IDs` used to create the cavity expansion object.
- The array `params` is a real array of parameters that is dependent on the model type. The array `params` is dimensioned so that it will hold all of the parameters used in the surface effects model. For the `SIMPLE_ON_OFF` model, there are four parameters:

  `param[0]`= free-surface top

  `param[1]`= free-surface bottom

  `param[2]`= free-surface top coefficient

  `param[3]`= free-surface bottom coefficient

See Section 2.4 for a description of the parameters for the `SIMPLE_ON_OFF` model.

3.3 Initializing the CavityExpansion Object

Cavity expansion must be initialized before calling `Compute_Forces` (Section 3.4) and after adding all of the surface effect models. The initialization phase connects the layers and the surface effect models, precomputes the expansion radii, and sets up the memory for the object that will be needed in `Compute_Forces`.

The prototype for the initialization is as follows:

```
CE_Error_Code
CavityExpansion::Initialize(
        const double* coordinates,
        const double* body_axis_points);
```

Definitions of the input parameters are given below.

- The real array `coordinates` is an array of initial coordinate positions ordered (*x*, *y*, *z*) for node 1, (*x*, *y*, *z*) for node 2, and so forth.
- The real array `body_axis_points` is an array of positions ordered (*x*, *y*, *z*) for body axis node 1, (*x*, *y*, *z*) for body axis node 2, and so forth.

3.4 Computing Nodal Forces

The nodal forces exerted by the target on the penetrator are computed in `Compute_Forces`. The prototype for this function is as follows:

```
CE_Error_Code
CavityExpansion::Compute_Forces(
        const double* coordinates,
        const double* velocities,
        const double* body_axis_points,
        double* forces );
```

Definitions of the input parameters are given below.

- The real array `coordinates` is an array of current nodal positions ordered (*x*, *y*, *z*) for node 1, (*x*, *y*, *z*) for node 2, and so forth.
- The real array `velocities` is an array of velocities ordered (*x*, *y*, *z*) for node 1, (*x*, *y*, *z*) for node 2, and so forth.
- The real array body_axis_points is an array of positions ordered (*x*, *y*, *z*) for body axis node 1, (*x*, *y*, *z*) for body axis node 2, and so forth.
- The real array `forces` contains the nodal forces exerted by the target on the penetrator nodes. The array `forces` is returned on exit from this function. Because the array is zeroed upon entering the function, the array CANNOT be used for accumulating the nodal forces.

4 Verification

This section describes the verification problems that are used to test the functionality of the CavityExpansion library. The current tests are listed below and discussed in detail in Section 4.1 through Section 4.7.

- Block with spherical expansion, constant pressure coefficient only
- Block with spherical expansion, constant pressure and linear velocity terms only
- Block with cylindrical expansion, constant pressure coefficient only
- Block with cylindrical expansion, constant pressure and linear velocity terms only
- Block with spherical expansion, constant pressure, multiple layers
- Block with cylindrical expansion, constant pressure, multiple layers
- Block with spherical expansion, constant pressure, top and bottom on-off surface effects

4.1 Block, Spherical CE, Constant Coefficient Only

This verification problem uses a block with an initial velocity. The block impacts the target and comes to rest after it penetrates the target by a certain distance due to a constant pressure from a spherical cavity expansion boundary condition.

4.1.1 Capabilities Tested

This problem tests spherical expansion with a constant pressure coefficient term only. Only the c_0 term in Equation (1) is nonzero. Calculation of the spherical normal and a constant pressure is tested.

Eight-node hexahedral elements and symmetry boundary conditions are used to define the numerical problem.

4.1.2 Mechanics of Problem

This problem uses a 1-inch $\times$ 1-inch $\times$ 1-inch block made of steel. Steel has a mass density of 7.324×10^{-4} lbm/in^3. The block has an initial velocity of 100 in/sec in the negative z-direction (Figure 4.1). The bottom of the block is initially at $z = 0$, and the top of the block is initially at $z = 1$. The block strikes the target at time $t = 0$. Only the constant term, c_0, in the quadratic equation used for cavity expansion is set to a nonzero value of 7.324 psi.

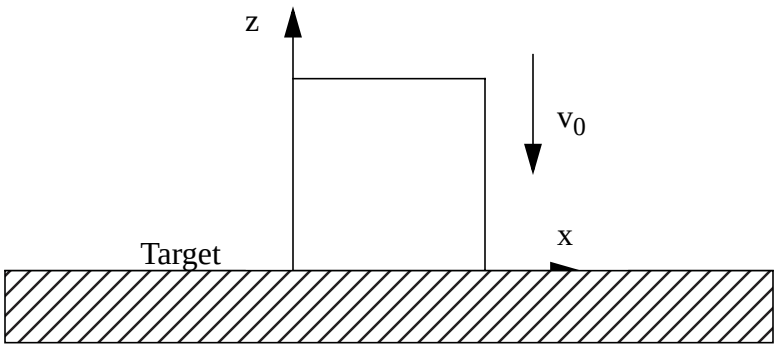

Figure 4.1. Block and target geometry.

The mesh used in this verification problem is a $2 \times 2 \times 2$ element block constructed of eight-node hexahedral elements. One edge of the block lies along the positive x-axis, one edge lies along the positive y-axis, and a third lies along the positive z-axis. There are planes of interior nodes at $x = 2/3$ inch, $y = 2/3$ inch, and $z = 2/3$ inch. The exterior faces of the elements are $2/3$ inch $\times$ $2/3$ inch, $1/3$ inch $\times$ $2/3$ inch, and $1/3$ inch $\times$ $1/3$ inch. The symmetry boundary condition $u_y = 0$ is used on the plane $x = 0$, and the symmetry boundary condition $u_x = 0$ is used on the plane $y = 0$.

4.1.3 Analytic Results

The result of setting only the constant term in the quadratic equation for cavity expansion to a nonzero value is a constant pressure over time on the bottom surface of the block. The acceleration of the block, once it strikes the target, can be easily computed from the equation

$$a = F/M, \tag{17}$$

where F is the force on the block due to the constant pressure term and M is the total mass of the block. By integrating Equation (17) with respect to time, one obtains the velocity of the block as a function of time as

$$v = v_0 + (F/M)t, \tag{18}$$

where v_0 is the initial velocity of the block. By integrating once more with respect to time, one obtains the displacement of the block as a function of time as

$$u = v_0 t + (F/M)(t^2/2), \tag{19}$$

where it is assumed that the initial displacement for any point on the block is zero. The block is at rest when the velocity v is zero. The time at which the block comes to rest is

$$t_f = -v_0(M/F). \tag{20}$$

Substituting the value for the time at which the velocity is zero, t_f, into Equation (19) gives the depth of penetration of the block into the the target.

For a block with unit dimensions, the total force on the block is 7.324 lb since the value for c_0 is 7.324 psi and the cross-sectional area of the block is $1\ \text{in}^2$. Since the block is steel with a mass density of 7.324×10^{-4} lbm/in^3, the total mass of the block is 7.324×10^{-4} lbm. The time at which the block comes to rest is 1×10^{-2} sec; the block penetrates the target to a depth of -0.5 inch.

4.1.4 Comparison of Analytic and Computed Results

The cross-sectional area of the block will deform slightly due to Poisson effects as the block contacts the target. However, this effect is very small, and the cross-sectional area of the block can be treated as constant ($1\ \text{in}^2$) over the period in which the block contacts the target and comes to rest. The block should follow the analytic behavior closely. Figure 4.2 shows the displacement as a function of time for any point on the block. For node 1 (located at $x = 0$, $y = 0$, and $z = 1$), the predicted displacement in the z-direction at time $t = 10.5 \times 10^{-3}$ sec is -0.499992 inch. This result is from Alegra. The numerical and analytic results show good agreement.

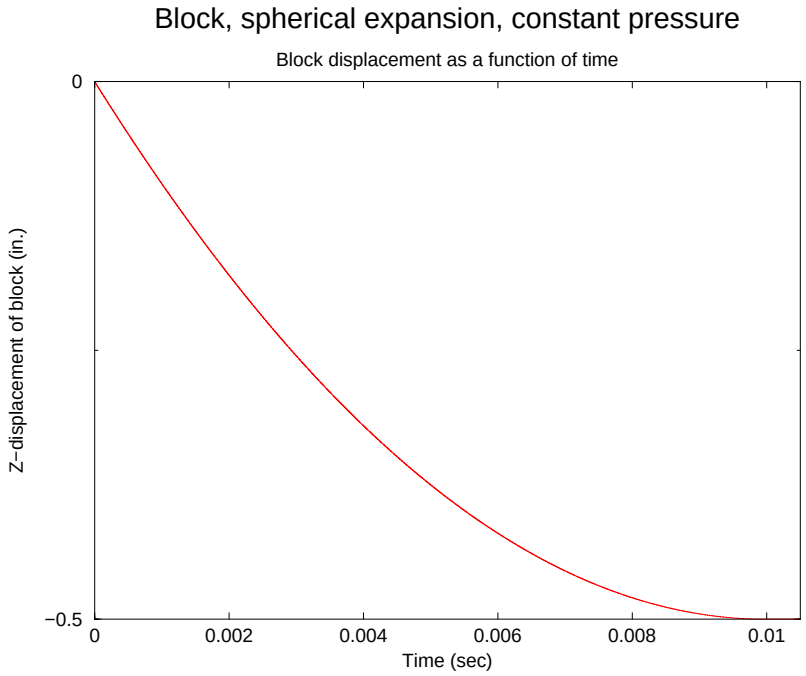

Figure 4.2. Displacement as a function of time for block impacting target; spherical expansion, constant pressure term only.

4.2 Block, Spherical CE, Constant and Linear Coefficients

This verification problem uses a block with an initial velocity. The block impacts the target and comes to rest after it penetrates the target by a certain distance due to a pressure from a spherical cavity expansion boundary condition. This problem is the same as the problem presented in Section 4.1, except that the pressure in this problem includes that due to the linear velocity term in addition to the constant pressure term.

4.2.1 Capabilities Tested

This problem tests spherical expansion with a constant coefficient pressure term and the pressure term that is linear in the velocity. Both the c_0 and c_1 terms in Equation (1) are nonzero for this problem; the c_2 term in Equation (1) is zero for this problem. Calculation of the spherical normal and the pressure with constant and linear terms is tested.

Eight-node hexahedral elements and symmetry boundary conditions are used to define the numerical problem.

4.2.2 Mechanics of Problem

The mechanics of this problem is the same as that for the problem presented in Section 4.1, except that this problem has a nonzero value for c_1 in addition to a nonzero value for c_0. The pressure on the block arises not only from the constant pressure term but also from the linear velocity term. The value for the coefficient c_1 is set to 0.07324 lb-sec/in^3.

4.2.3 Analytic Results

For this particular verification problem, the motion of the block is described by the differential equation

$$M\frac{d^2u}{dt^2} = -c_0 - c_1\frac{du}{dt}, \tag{21}$$

where M is the total mass of the block and u is the displacement of the block. Since we are working with unit areas for the surface of the block, the terms on the right-hand side in Equation (21) represent force terms. Equation (21) is rewritten is a differential equation with the homogeneous solution

$$u = Ae^{(-c_1/M)t} \tag{22}$$

and the particular solution

$$u = (-c_0/c_1)t + A_0, \tag{23}$$

where A and A_0 are constants determined from initial conditions. The initial conditions are that the displacement of the block is zero and the initial velocity is v_0 at $t = 0$. The initial conditions yield

$$A = -(v_0 + c_0/c_1)/(M/c_1) \tag{24}$$

and

$$A_0 = -A, \tag{25}$$

which results in

$$u = (v_0 + c_0/c_1)/(M/c_1)(1 - e^{(-c_1/M)t}) - (c_0/c_1)t \tag{26}$$

as the expression for the displacement as a function of time. The block is at rest when

$$\frac{du}{dt} = 0, \tag{27}$$

which occurs at time

$$t_f = -\left(\frac{M}{c_1}\right)\ln\left(\frac{c_0/c_1}{v_0 + c_0/c_1}\right). \tag{28}$$

By substituting the value for t_f into Equation (26), one can obtain the displacement for the block at the point where it is at rest in the target.

For a total mass of 1 lbm, an initial velocity of 100 in/sec in the minus *z*-direction, and values of 7.324 lb/in^2 and 0.07324 lb-sec/in^3 for c_0 and c_1, respectively, the time at which the block comes to rest is 6.9315×10^{-3} sec. The block penetrates the target to a depth of -3.0685×10^{-1} inch.

4.2.4 Comparison of Analytic and Computed Results

The cross-sectional area of the block will deform slightly due to Poisson effects as the block contacts the target. However, this effect is very small, and the cross-sectional area of the block can be treated as constant (1 in^2) over the period in which the block contacts the target and comes to rest. The block should follow the analytic behavior closely. Figure 4.3 shows the displacement as a function of time for any point on the block. For node 1 (located at $x = 0$, $y = 0$, $z = 1$), the predicted displacement in the *z*-direction at the time the block comes to rest ($t = 10.5 \times 10^{-3}$ sec) is $-3.0667979 \times 10^{-1}$ inch. This result is from Alegra. The numerical and analytic results show good agreement (within 0.055%).

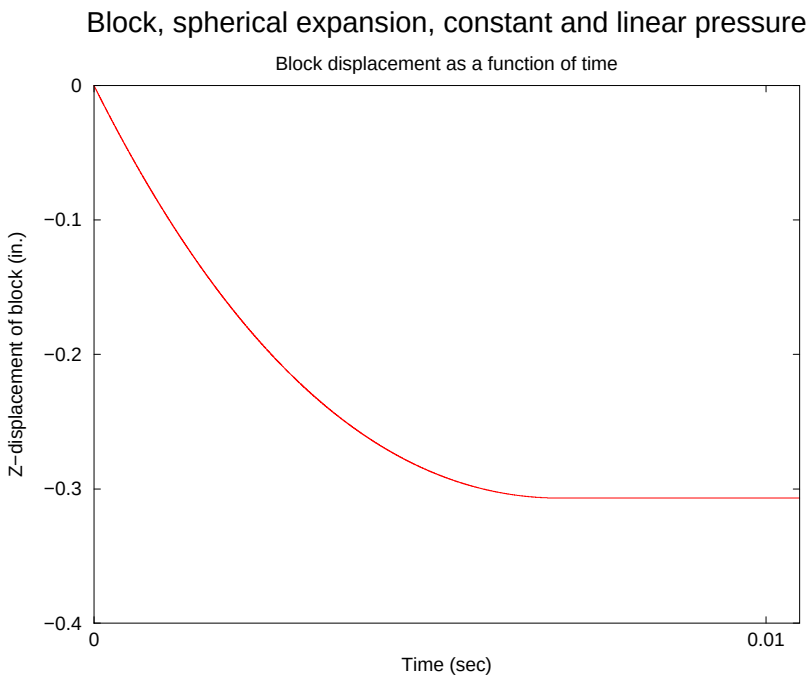

Figure 4.3. Displacement as a function of time for block impacting target; spherical expansion, constant pressure and linear velocity terms only.

4.3 Block, Cylindrical CE, Constant Coefficient Only

This verification problem uses a block with an initial velocity in the *x*-direction. The block is embedded in the target and comes to rest after a certain distance due to a constant pressure from a cylindrical cavity expansion boundary condition. The nature of cylindrical expansion requires that the block be embedded in the target and moved in a direction orthogonal to the *z*-axis, which is the assumed target normal.

4.3.1 Capabilities Tested

This problem tests cylindrical expansion with a constant pressure coefficient term only. Only the c_0 term in Equation (1) is nonzero. Calculation of the cylindrical normal and a constant pressure is tested.

Eight-node hexahedral elements and symmetry boundary conditions are used to define the numerical problem.

4.3.2 Mechanics of Problem

This problem uses a 1-inch $\times$ 1-inch $\times$ 1-inch block made of steel. Steel has a mass density of 7.324×10^{-4} lbm/in^3. The block has an initial velocity of 100 in/sec in the positive x-direction. The bottom of the block is initially at $z = 0$, and the top of the block is initially at $z = 1$. The top of the target is at $z = 10$ inches, and the bottom of the target is at $z = -10$ inches. The block is embedded in the target. A pressure is applied to the block in the minus x-direction beginning at time zero due to cylindrical cavity expansion. Only the constant term, c_0, in the quadratic equation used for cavity expansion is set to a nonzero value; the constant term is set to 7.3324 psi.

The mesh used in this verification problem is a $2 \times 2 \times 2$ element block constructed of eight-node hexahedral elements. One edge of the block lies along the positive x-axis, one edge lies along the positive y-axis, and a third lies along the positive z-axis. There are planes of interior nodes at $x = 2/3$ inch, $y = 2/3$ inch, and $z = 2/3$ inch. The exterior faces of the elements are $2/3$ inch $\times$ $2/3$ inch, $1/3$ inch $\times$ $2/3$ inch, and $1/3$ inch $\times$ $1/3$ inch. The symmetry boundary condition $u_y = 0$ is used on the plane $x = 0$, and the symmetry boundary condition $u_z = 0$ is used on the plane $z = 1$. Node 7, which is located at $x = 1$, $y = 0$, and $z = 1$, is used to track the motion of the block.

4.3.3 Analytic Results

The result of setting only the constant term in the quadratic equation for cavity expansion to a nonzero value is a constant pressure over time on the surface of the block with a normal in the x-direction. The acceleration of the block beginning at time $t = 0$ can be easily computed from the equation

$$a = F/M, \tag{29}$$

where F is the force on the block due to the constant pressure term and M is the total mass of the block. By integrating Equation (29) with respect to time, one obtains the velocity of the block as a function of time as

$$v = v_0 + (F/M)t, \tag{30}$$

where v_0 is the initial velocity of the block. By integrating once more with respect to time, one obtains the displacement of the block as a function of time as

$$u = v_0 t + (F/M)(t^2/2), \tag{31}$$

where it is assumed that the initial displacement for any point on the block is zero. The block is at rest when the velocity v is zero. The time at which the block comes to rest is

$$t_f = -v_0(M/F). \tag{32}$$

Substituting the value for the time at which the velocity is zero, t_f, into Equation (32) gives the depth of penetration of the block into the the target.

For a block with unit dimensions, the total force on the block is 7.324 lb since the value for c_0 is 7.324 psi and the cross-sectional area of the block is $1\ \text{in}^2$. Since steel has a mass density of 7.324×10^{-4} lbm/in^3, the total mass of the block is 7.324×10^{-4} lbm. The time at which the block comes to rest is 1×10^{-2} sec; the block moves a distance of 0.5 inch through the target in the *x*-direction.

4.3.4 Comparison of Analytic and Computed Results

The cross-sectional area of the block will deform slightly due to Poisson effects as the block moves through the target. However, this effect is very small, and the cross-sectional area of the block can be treated as constant ($1\ \text{in}^2$) over the period in which the block is moving through the target. The block should follow the analytic behavior closely. Figure 4.4 shows the displacement as a function of time for any position on the block. For node 7 (located at $x = 1$, $y = 0$, $z = 1$), the predicted displacement at time $t = 10.5 \times 10^{-3}$ sec is 0.499990 inch. This result is from Alegra. The numerical and analytic results show good agreement.

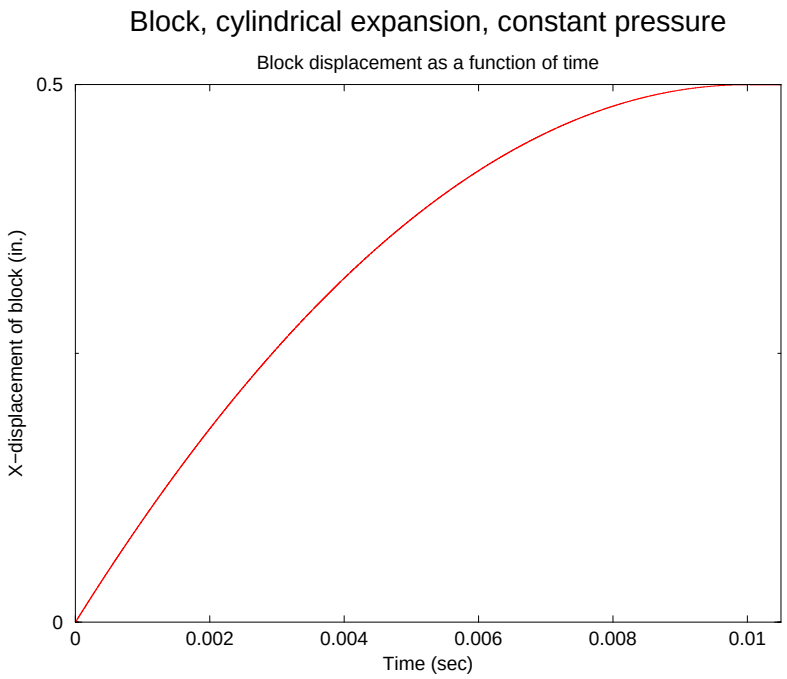

Figure 4.4. Displacement as a function of time for block moving through target; cylindrical expansion, constant pressure term only.

4.4 Block, Cylindrical CE, Constant and Linear Coefficients

This verification problem uses a block with an initial velocity in the *x*-direction. The block is embedded in the target and comes to rest after a certain distance due to a pressure from a cylindrical cavity expansion boundary condition. This problem is the same as the problem presented in Section 4.3, except that the pressure in this problem includes that due to the linear velocity term in addition to the constant pressure term. The nature of cylindrical expansion requires that the block be embedded in the target and moved in a direction orthogonal to the *z*-axis, which is the assumed target normal.

4.4.1 Capabilities Tested

This problem tests cylindrical expansion with a constant pressure coefficient and the pressure term that is linear in the velocity. Both the c_0 and c_1 terms in Equation (1) are nonzero for this problem; the c_2 term in Equation (1) is zero for this problem. Calculation of the spherical normal, the cylindrical normal, and the pressure with constant and linear terms is tested.

Eight-node hexahedral elements and symmetry boundary conditions are used to define the numerical problem.

4.4.2 Mechanics of Problem

The mechanics of this problem is similar to that for the problem presented in Section 4.3, except that this problem has a nonzero value for c_1 in addition to a nonzero value for c_0. The pressure on the block arises not only from the constant pressure term but also from the linear velocity term. The determination of the pressure due to the linear velocity term is slightly more complicated than that for the analogous spherical cavity expansion problem described in Section 4.2. To determine the pressure arising from the linear velocity term, consider the block geometry with normals shown in Figure 4.5.

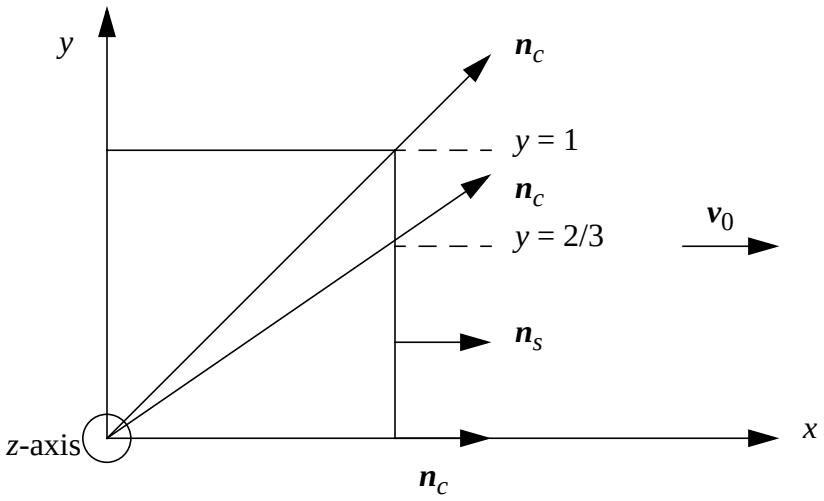

Figure 4.5. Normals for block for cylindrical expansion.

The velocity v used to calculate the pressure from the velocity at the node $\boldsymbol{v}_n$ is given by

$$v = \boldsymbol{v}_n \cdot \boldsymbol{n}_s / (\boldsymbol{n}_s \cdot \boldsymbol{n}_c), \tag{33}$$

where $\boldsymbol{n}_s$ is the spherical normal at the node and $\boldsymbol{n}_c$ is the cylindrical normal at the node. For this particular problem, the body axis for the block lies along the z-axis. Although the spherical normals are all the same for the faces of interest for this problem (1, 0, 0), the cylindrical normals vary with the location of the nodes. For the nodes located at $y = 0$, the cylindrical normals of interest are (1, 0, 0), and the product $\boldsymbol{n}_c \cdot \boldsymbol{n}_s$ is 1.0. For the nodes located at $y = 2/3$, the cylindrical normals of interest are $(1/\sqrt{13/9},\ 2/3/\sqrt{13/9},\ 0)$, and the product $\boldsymbol{n}_c \cdot \boldsymbol{n}_s$ is $1/\sqrt{13/9}$. For the nodes located at $y = 1$, the cylindrical normals of interest are $(\sqrt{2}/2,\ \sqrt{2}/2,\ 0)$, and the product $\boldsymbol{n}_c \cdot \boldsymbol{n}_s$ is $\sqrt{2}/2$. If v_x is the velocity along the face at $x = 1$ at any instant, we can approximate the pressure along this face as a function of y with a simple quadratic as

$$p = c_1 v_x (0.33431 y^2 + 0.079905 y + 1.0). \tag{34}$$

If we integrate the function for pressure over the face of the block normal to the *x*-direction from $y = 0$ to $y = 1$ and from $z = 0$ to $z = 1$, then the total force on the block normal to the *x*-direction is $F_x = 1.15139 c_1 v_x$.

If the value of the coefficient c_1 is set to $0.07324/1.15139$, which is 0.063610, then the force in the *x*-direction as a function of time will be the same as that for the spherical expansion problem in Section 4.2, and the behavior for this problem will be the same as that for the problem in Section 4.2. For the problem in Section 4.2, the value for c_1 is 0.07324 lb-sec/in^3.

4.4.3 Analytic Results

For this particular verification problem, the motion of the block is described by the differential equation

$$M \frac{d^2 u}{dt^2} = -c_0 - c_1 \frac{du}{dt}, \tag{35}$$

where *M* is the total mass of the block and *u* is the displacement of the block. Since we are working with unit areas for the surface of the block, the terms on the right-hand side in Equation (35) represent force terms. As indicated in the previous section, however, the value for c_1 must be adjusted to account for the geometry and configuration of the cylindrical normals in order to use $c_1 \frac{du}{dt}$ directly as a force term. Equation (35) is rewritten is a differential equation with the homogeneous solution

$$u = A e^{(-c_1/M)t} \tag{36}$$

and the particular solution

$$u = (-c_0/c_1)t + A_0, \tag{37}$$

where *A* and A_0 are constants determined from initial conditions. The initial conditions are that the displacement of the block is zero and the initial velocity is v_0 at $t = 0$. The initial conditions yield

$$A = -(v_0 + c_0/c_1)/(M/c_1) \tag{38}$$

and

$$A_0 = -A, \tag{39}$$

which results in

$$u = (v_0 + c_0/c_1)/(M/c_1)(1 - e^{(-c_1/M)t}) - (c_0/c_1)t \tag{40}$$

as the expression for the displacement as a function of time. The block is at rest when

$$\frac{du}{dt} = 0, \tag{41}$$

which occurs at time

$$t_f = -\left(\frac{M}{c_1}\right)\ln\left(\frac{c_0/c_1}{v_0 + c_0/c_1}\right). \tag{42}$$

By substituting the value for t_f into Equation (40), one can obtain the displacement for the block at the point where it is at rest in the target.

For a total mass of 1 lbm, an initial velocity of 100 in/sec in the minus z-direction, and values of 7.324 psi and 0.063610 lb-sec/in^3 for c_0 and c_1, respectively, the time at which the block comes to rest is 6.9315×10^{-3} sec. The block moves through the target a distance of -3.0685×10^{-1} inch.

4.4.4 Comparison of Analytic and Computed Results

The cross-sectional area of the block will deform slightly due to Poisson effects as the block moves through the target. However, this effect is very small, and the cross-sectional area of the block can be treated as constant (1 in^2) over the period in which the block is moving through the target. The block should follow the analytic behavior closely. Figure 4.6 shows the displacement for any point as a function of time for any point on the block. For node 7 (located at $x = 1$, $y = 0$, $z = 1$), the predicted displacement at time $t = 10.5 \times 10^{-3}$ sec is 0.3049608 inch. This result is from Alegra. The numerical and analytic results show good agreement.

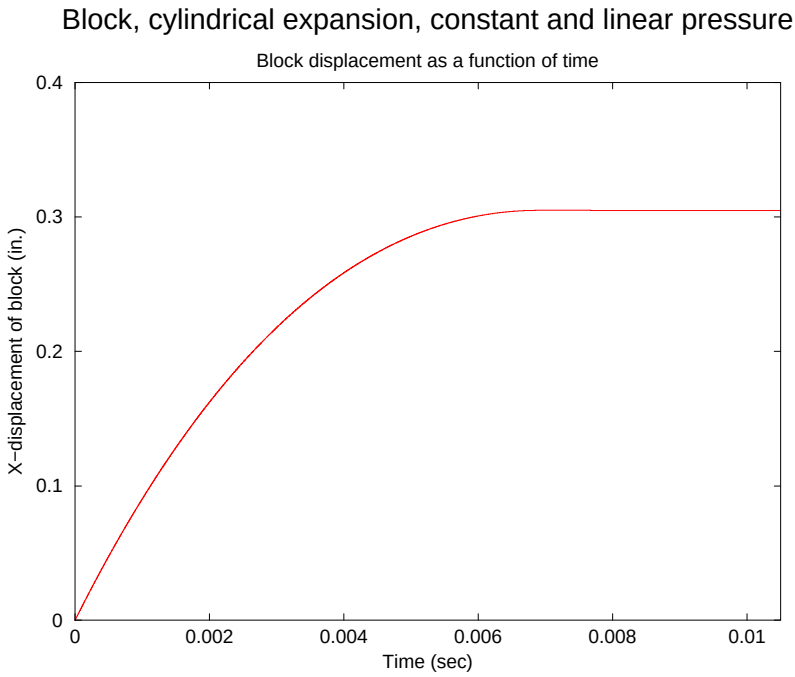

Figure 4.6. Displacement as a function of time for block moving through target; cylindrical expansion, constant pressure and linear velocity terms only.

4.5 Block, Spherical CE, Constant Coefficients, Multiple Layers

This verification problem uses a block with an initial velocity. The block impacts the target and comes to rest after it penetrates the target by a certain distance due to a pressure from a spherical cavity expansion boundary condition. This problem is the same as the one described in Section 4.1, except that the problem in this section (Section 4.5) uses three layers rather than one layer to describe the layer structure inside the target. For this particular problem, all layers have the same properties. The behavior for this problem is exactly the same as that for the problem in Section 4.1.

4.5.1 Capabilities Tested

This problem tests spherical expansion with a constant pressure coefficient only and multiple layers inside the target. Calculation of the spherical normal and the pressure for a multilayer problem is tested.

Eight-node hexahedral elements and symmetry boundary conditions are used to define the numerical problem.

4.5.2 Mechanics of Problem

The mechanics for this problem is the same as that defined in Section 4.1.2, except that this problem uses three layers instead of one inside the target. For all layers, the value for c_0 is 7.324 psi.

The layers range from $z = 0.0$ inch to $z = -0.2$ inch, from $z = -0.2$ inch to $z = -0.4$ inch, and from $z = -0.4$ inch to $z = -0.6$ inch. The block passes completely through the first two layers and comes to rest in the third layer ranging from $z = -0.4$ inch to $z = -0.6$ inch.

4.5.3 Analytic Results

The analytic results for this problem can be obtained by using the results in Section 4.1.3.

4.5.4 Comparison of Analytic and Computed Results

Computed results for this problem compare to the results shown in Figure 4.2. For node 1 (located at $x = 0, y = 0, z = 1$), the predicted displacement in the *z*-direction at time $t = 10.5 \times 10^{-3}$ sec is -0.499992 inch. This result is from Alegra. The numerical and analytic results show good agreement.

4.6 Block, Cylindrical CE, Constant Coefficients, Multiple Layers

This verification problem uses a block with an initial velocity. The block moves through the target and comes to rest after a certain distance due to a pressure from a spherical cavity expansion boundary condition. This problem is the same as the one described in Section 4.3, except that the problem in this section (Section 4.6) uses two layers rather than one layer to describe the layer structure inside the target. For this particular problem, both layers have the same properties. The behavior for this problem is exactly the same as that for the problem in Section 4.3.

4.6.1 Capabilities Tested

This problem tests cylindrical expansion with a constant pressure coefficient only and multiple layers inside the target. Calculation of the spherical normal and the pressure for a multilayer problem is tested.

Eight-node hexahedral elements and symmetry boundary conditions are used to define the numerical problem.

4.6.2 Mechanics of Problem

The mechanics for this problem is the same as that defined in Section 4.3.2, except that this problem uses two layers instead of one layer inside the target. For both layers, the value for c_0 is 7.324 psi.

The layers range from $z = 2.0$ inches to $z = 0.5$ inch and from $z = 0.5$ inch to $z = -2.0$ inches. Since the top of the block is at $z = 1.0$ inch and the bottom of the block is at $z = 0.0$ inch, the block is in both layers. The block remains in both layers since the motion of the block is in the *x*-direction.

4.6.3 Analytic Results

The analytic results for this problem can be obtained by using the results in Section 4.3.3.

4.6.4 Comparison of Analytic and Computed Results

Computed results for this problem compare to the results shown in Figure 4.4. For node 7 (located at $x = 1$, $y = 0$, $z = 1$), the predicted displacement in the *x*-direction at time $t = 10.5 \times 10^{-3}$ sec is 0.499990 inch. This result is from Alegra. The numerical and analytic results show good agreement.

4.7 Block, Spherical CE, Constant Pressure, Surface Effects

This verification problem uses a block with an initial velocity. The block impacts the target and experiences a constant pressure due to a cavity expansion boundary condition. Only the c_0 term in Equation (1) is nonzero. A surface effect coefficient, the scale factor f_s in Equation (15), is specified for a top on-off surface effect and for a bottom on-off surface effect. The top surface effect coefficient does not influence the motion of the block as it impacts the surface because the normals for the faces on the bottom of the block are opposite to the surface normal for the target. For the on-off surface effect to be enforced for a given face, the normal to the face and the target surface normal of interest (lower- or upper-target surface normal) must first have components in the same direction. The bottom surface of the target and the bottom surface effect coefficient are set so that the bottom surface effect does influence the motion of the block. The bottom surface effect is such that, at some depth of penetration of the block, the bottom surface effect turns off the pressure on the block, and the block continues its motion at a constant velocity.

4.7.1 Capabilities Tested

This problem tests spherical expansion with a constant pressure coefficient only and top and bottom surface effects.

Eight-node hexahedral elements and symmetry boundary conditions are used to define the numerical problem.

4.7.2 Mechanics of Problem

This problem uses a 1-inch $\times$ 1-inch $\times$ 1-inch block made of steel. Steel has a mass density of 7.324×10^{-4} lbm/in^3. The block has an initial velocity of 100 in/sec in the negative z-direction. The bottom of the block is initially at $z = 0$, and the top of the block is initially at $z = 1$. The block strikes the target at time $t = 0$. Only the constant term, c_0, in the quadratic equation used for cavity expansion is set to a nonzero value; the constant term is set to 7.324 psi.

A value of 10.0 is used to specify the scale factor for the top surface effect. The top surface effect never influences the motion of the block because the normals on the bottom surface of the block (which are given by (0, 0, –1)) are in the opposite direction of the normal to the top surface of the target, which is given by (0, 0, 1). A value of 10.0 is also used to specify the scale factor for the bottom surface effect. The bottom surface of the target is set to $z = -10$ inches, and the bottom of the layer in the target is set at $z = -0.5$ inch. The tip radius is set to 0.01 inch. When the bottom surface of the block has penetrated to a depth of $z = -0.4$ inch, the bottom surface effect turns off the constant pressure term. The distance l (see Section 2.4) to the bottom of the layer when $z = -0.4$ inch is 0.1 inch. The scale factor of the bottom surface effect, f_s, times the tip radius, r, gives a value of 0.1 inch ($f_s r = 10.0 \times 0.01$ inch). Once the block displacement is greater than $z = -0.4$, the relation given in Equation (15) of Section 2.4 ($l - f_s r > 0$) is no longer satisfied, and the pressure due to cavity expansion is set to zero. The velocity at this point remains constant, and the displacement of any point on the block is described by a linear function.

The mesh used in this verification problem is a $2 \times 2 \times 2$ element block constructed of eight-node hexahedral elements. One edge of the block lies along the positive x-axis, one edge lies along the positive y-axis, and a third lies along the positive z-axis. There are planes of interior nodes at $x = 2/3$ inch, $y = 2/3$ inch, and $z = 2/3$ inch. The exterior faces of the elements are $2/3$ inch $\times$ $2/3$ inch, $1/3$ inch $\times$ $2/3$ inch, and $1/3$ inch $\times$ $1/3$ inch. The symmetry boundary condition $u_y = 0$ is used on the plane $x = 0$, and the symmetry boundary condition $u_x = 0$ is used on the plane $y = 0$.

4.7.3 Analytic Results

The result of setting only the constant term in the quadratic equation for cavity expansion to a nonzero value is a constant pressure over time on the bottom surface of the block. The acceleration of the block, once it strikes the target, can be easily computed from the equation

$$a = F/M, \tag{43}$$

where F is the force on the block due to the constant pressure term and M is the total mass of the block. By integrating Equation (43) with respect to time, one obtains the velocity of the block as a function of time as

$$v = v_0 + (F/M)t, \tag{44}$$

where v_0 is the initial velocity of the block. By integrating once more with respect to time, one obtains the displacement of the block as a function of time as

$$u = v_0 t + (F/M)(t^2/2), \tag{45}$$

where it is assumed that the initial displacement for any point on the block is zero. The pressure on the block becomes zero when the block penetrates the target by a certain depth u_b because of the bottom surface effect. The time t_b at which u_b is reached is the appropriate root of

$$t_b = \frac{-v_0 \pm \sqrt{v_0^2 + 2Fu_b/M}}{F/M}. \tag{46}$$

The final velocity for the block is

$$v_b = v_0 + (F/M)t_b, \tag{47}$$

and the displacement of the block for any time $t > t_b$ is

$$u = u_b + v_b(t - t_b). \tag{48}$$

For this particular problem, the block displaces by 0.4 inch into the target at time $t = 5.522786 \times 10^{-3}$ sec and has a velocity of $v = -44.7214$ in/sec. By using Equation (48), the predicted displacement at time $t = 10.5 \times 10^{-3}$ sec, the termination time for the problem, should be -0.622236 inch.

4.7.4 Comparison of Analytic and Computed Results

The cross-sectional area of the block will deform slightly due to Poisson effects as the block contacts the target. However, this effect is very small, and the cross-sectional area of the block can be treated as constant ($1\ \text{in}^2$) over the period in which the block contacts the target and comes to rest. The block should follow the analytic behavior closely. Figure 4.7 shows the displacement as a function of time for any point on the block. For node 1 (located at $x = 1$, $y = 0$, $z = 1$), the predicted velocity when the block penetrates to a

depth of –0.4 inch is –44.7203 in/sec. For node 1, the predicted displacement in the *z*-direction at time $t = 10.5 \times 10^{-3}$ sec is –0.62239 inch. This result is from Alegra. The numerical and analytic results show good agreement.

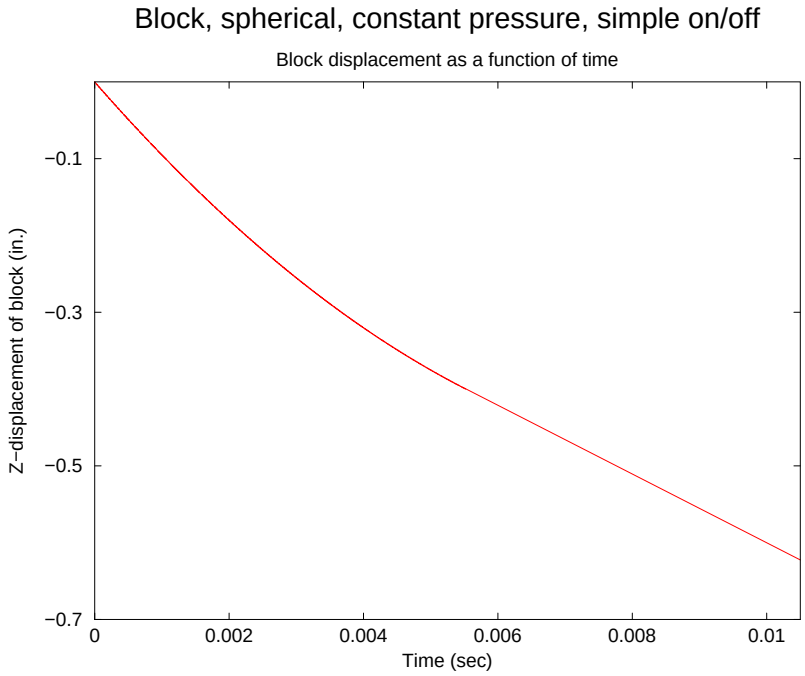

Figure 4.7. Displacement as a function of time for block impacting target; spherical expansion, constant pressure term only, simple on-off surface effects.

5 Validation

Cavity expansion has been validated as an analysis tool by comparing numerical and experimental results for a number of problems. Validation results are given in References 11, 14, 15, and 16.

References

1. *ABAQUS Users Manual*, Version 4-8. Providence, RI: Hibbitt, Karlsson, and Sorenson, Inc., 1989.

2. Bishop, R. F., and N. F. Mott. “The Theory of Indentation and Hardness.” *Proceedings of the Royal Society* 57, no. 3 (1945): 147–159.

3. Boucheron, E. A., K. H. Brown, K. G. Budge, D. E. Carroll, S. K. Carroll, M. A. Christon, R. R. Drake, C. G. Garasi, T. A. Haill, J. S. Peery, S. V. Petney, J. Robbins, A. C. Robinson, R. M. Summers, J. R. Weatherby, and M. K. Wong. *Alegra: User Input and Physics Descriptions*, SAND2001-1992. Albuquerque, NM: Sandia National Laboratories, 2001.

4. Forrestal, M. J., and D. Y. Tzou. “A Spherical Cavity-Expansion Penetration Model for Concrete Targets.” *International Journal of Solids and Structures* 34, no. 31–32 (1997): 4217–4146.

5. Goodier, J. N. “On the Mechanics of Indentation and Cratering in the Solid Targets of Strain-Hardening Metal by Impact of Soft Spheres.” In *Proceedings of the 7th Symposium on Hypervelocity Impact III*, 215–259. New York: AIAA, 1965.

6. Hill, R. *The Mathematical Theory of Plasticity.* London: Oxford University Press, 1950.

7. Hopkins, H. G. “Dynamic Expansion of Spherical Cavities in Metals.” In *Progress in Solid Mechanics*, Vol. 1, edited by I. Sneddon and R. Hill, 85–164. New York: North Holland, 1960.

8. Koteras, J. R., A. S. Gullerud, V. L. Porter, W. M. Scherzinger, and K. H. Brown. “PRESTO: Impact Dynamics with Scalable Contact Using the SIERRA Framework.” In *Proceedings of the First MIT Conference on Computational Fluid and Solid Mechanics*, Massachusetts Institute of Technology, Cambridge, MA. Amsterdam: Elsevier, June 2001.

9. Longcope, D. B., and M. J. Forrestal. “Penetration of Targets Described by a Mohr-Coulomb Failure Criterion with a Tension Cutoff.” *Journal of Applied Mechanics* 50 (1983): 327–333.

10. Longcope, D. B. *Coupled Bending/Lateral Load Modeling of Earth Penetrators*, SAND91-0789. Albuquerque, NM: Sandia National Laboratories, 1991.

11. Longcope, D. B. *Oblique Penetration Modeling and Correlation with Field Tests into a Soil Target*, SAND96-2239. Albuquerque, NM: Sandia National Laboratories, 1996.

12. Longcope, D. B., M. R. Tabbara, and J. Jung. *Modeling of Oblique Penetration into Geologic Targets Using Cavity Expansion Penetrator Loading with Target Free-Surface Effects,* SAND99-1104. Albuquerque, NM: Sandia National Laboratories, 1999.

13. Taylor, L. M., and D. P. Flanagan. *Pronto3d: A Three-Dimensional Transient Solid Dynamics Program,* SAND87-1912. Albuquerque, NM: Sandia National Laboratories, 1989.

14. Warren, T. L. “Simulations of the Penetration of Limestone Targets by Ogive-Nose 4340 Steel Projectiles.” *International Journal of Impact Engineering* 27 (2002): 475–496.

15. Warren, T. L., and K. L. Poormon. “Penetration of 6061-T6511 Aluminum Targets by Ogive-Nosed VAR 4340 Steel Projectiles at Oblique Angles: Experiments and Simulations.” *International Journal of Impact Engineering* 25 (2001): 993–1022.

16. Warren, T. L., and M. R. Tabbara. *Spherical Cavity-Expansion Forcing Function in Pronto3d for Application to Penetration Problems*, SAND97-1174. Albuquerque, NM: Sandia National Laboratories, 1997.

Appendix A: Basic Algorithmic Flow

The basic algorithmic flow used for the implementation of cavity expansion is given below.

```
Collect input information
  Type of cavity expansion (spherical or cylindrical)
  Target normal axis (X, Y, or Z)
  Free surface top location
  Free surface bottom location
  Layer surface top location
  Layer surface bottom location
  Pressure coefficients c0, c1, c2
  body axis point 1
  body axis point 2

Compute current body axis orientation: A = p1 - p2

Loop over faces defining surface with cavity expansion
effects

Collect information for nodes defining faces

Compute spherical normal to face

Loop over nodes defining face

  pressure = 0.0

  If node is within layer

    Vs = v dot ns

    If SPHERICAL cavity expansion

      If Vs > tolerance

        pressure = c0 + c1 Vs + c2 Vs Vs

        If top surface effect = true and normal pointing to
        top free surface

          If l/r < fs, pressure = 0

        Endif test on top free surface

        If bottom surface effect = true and normal pointing
        to bottom free surface

          If l/r < fs, pressure = 0

        Endif test on bottom free surface

      Endif test on Vs
    Endif test for SPHERICAL expansion

    If CYLINDRICAL cavity expansion
```

```
        Compute Vc

        Comnpute dot_normals = nc dot ns

        If dot_normals > tolerance

          Vc = Vs x dot_normals

          If Vc > tolerance

            pressure = c0 + c1 Vc + c2 Vc Vc

            If top surface effect = true and normal pointing
            to top free surface

            If l/r < fs, pressure = 0

            Endif test on top free surface

            If bottom surface effect = true and normal
            pointing to bottom free surface

            If l/r < fs, pressure = 0

            Endif test on bottom free surface

          Endif test on Vc

        Endif test on dot_normals

      Endif test for CYLINDRICAL expansion

    Endif test to determine node in layer

  End loop over nodes on face

  Calculate nodal forces at each node on face from pressure
  distribution.

  End loop over faces

  Sum element node forces into global force array

  End cavity expansion calculations.
```

Distribution

Scott W. Doebling
Los Alamos National Laboratory
PO Box 1663 MS P946
Los Alamos, NM 87545

Internal

1	MS-0318	P. Yarrington, 9230
1	MS-0321	W. J. Camp, 9200
1	MS-0427	J. R. Weatherby, 2134
1	MS-0521	S. T. Montgomery, 2561
1	MS-0807	B. Cole, 9338
1	MS-0819	W. J. Bohnhoff, 9231
10	MS-0819	K. H. Brown, 9231
1	MS-0819	S. P. Burns, 9231
1	MS-0819	D. E. Carroll, 9231
1	MS-0819	S. Carroll, 9231
1	MS-0819	M. A. Christon, 9231
1	MS-0819	R. R. Drake, 9231
1	MS-0819	C. J. Garasi, 9231
1	MS-0819	D. M. Hensinger, 9231
1	MS-0819	S. V. Petney, 9231
1	MS-0819	J. Robbins, 9231
1	MS-0819	A. C. Robinson, 9231
1	MS-0819	R. M. Summers, 9231
1	MS-0819	T. G. Trucano, 9211
1	MS-0819	T. E. Voth, 9231
1	MS-0819	M. K. Wong, 9231
1	MS-0826	J. S. Rath, 9143
1	MS-0826	J. R. Stewart, 9143
1	MS-0826	J. D. Zepper, 9143
1	MS-0827	H. C. Edwards, 9143
1	MS-0827	M. E. Hamilton, 9143
1	MS-0827	T. J. Otahal, 9143
1	MS-0834	A. C. Ratzel, 9110
1	MS-0834	P. R. Schunk, 9114
1	MS-0835	K. F. Alvin, 9142
1	MS-0835	E. A. Boucheron, 9141
1	MS-0835	S. W. Bova, 9141
1	MS-0835	N. K. Crane, 9142
1	MS-0835	R. R. Lober, 9141
1	MS-0835	J. M. McGlaun, 9140

1	MS-0835	K. H. Pierson, 9142
1	MS-0835	T. F. Walsh, 9142
1	MS-0841	T. C. Bickel, 9100
1	MS-0847	C. R. Adams, 9125
1	MS-0847	S. W. Attaway, 9134
1	MS-0847	M. K. Bhardwaj, 9142
1	MS-0847	F. Bitsie, 9124
1	MS-0847	M. L. Blanford, 9142
1	MS-0847	S. N. Burchett, 9126
1	MS-0847	H. Duong, 9126
1	MS-0847	C. W. Fulcher, 9125
1	MS-0847	K. W. Gwinn, 9126
1	MS-0847	A. S. Gullerud, 9142
1	MS-0847	T. D. Hinnerichs, 9126
1	MS-0847	J. Jung, 9127
1	MS-0847	S. W. Key, 9142
10	MS-0847	J. R. Koteras, 9142
1	MS-0847	J. S. Lash, 9126
10	MS-0847	D. B. Longcope, 9127
1	MS-0847	R. A. May, 9126
1	MS-0847	K. E. Metzinger, 9126
1	MS-0847	J. A. Mitchell, 9142
1	MS-0847	H. S. Morgan, 9120
1	MS-0847	V. L. Porter, 9142
1	MS-0847	G. M. Reese, 9142
1	MS-0847	G. D. Sjaardema, 9143
1	MS-0847	C. M. Stone, 9142
1	MS-0847	J. W. Swegle, 9142
1	MS-0893	M. K. Neilsen, 9123
1	MS-0893	W. M. Scherzinger, 9123
1	MS-0893	G. W. Wellman, 9123
1	MS-1110	D. E. Womble, 9214
1	MS-1111	K. D. Devine, 9226
1	MS-1111	C. T. Vaughan, 9224
1	MS-1164	J. L. McDowell, 15400
1	MS-1174	W. H. Rutledge, 15414
10	MS-1174	T. L. Warren, 15414
1	MS-1185	J. Pott, 15417
1	MS-9001	J. L. Handrock, 1843
1	MS-9042	J. Crowell, 8727
1	MS-9042	J. Dike, 8727
1	MS-9042	R. Gilbert-O’Neil, 8727
1	MS-9042	P. M. Gullett, 8727

1	MS-9042	B. Kistler, 8727
1	MS-9042	C. Moen, 8728
1	MS-9042	V. Revelli, 8727
1	MS-9042	P. A. Spence, 8727
1	MS-9161	E-P Chen, 8726
1	MS-9161	P. A. Klein, 8726
1	MS-9018	Central Technical Files, 8945-1
2	MS-0899	Technical Library, 9616
2	MS-0612	Review and Approval Desk, 9612, For DOE OSTI